

Using Deep Learning to Bootstrap Abstractions for Hierarchical Robot Planning

Naman Shah
Arizona State University
Tempe, USA
namanshah@asu.edu

Siddharth Srivastava
Arizona State University
Tempe, USA
siddharths@asu.edu

ABSTRACT

Autonomous robots need to be able to efficiently compute long-horizon motion plans for achieving user desired tasks. Hierarchical planning approaches address this problem but require input state and action abstractions to decompose the overall problem and guide motion planners. This paper presents a new approach for bootstrapping the entire abstraction process by learning to predict the critical regions of a configuration space, using them to construct high-level actions as transitions between critical regions, and finally, by using the discovered actions to efficiently compute long-horizon motion plans. In this process, it auto-generating robot-specific deep neural network architectures for predicting high-dimensional critical regions in the configuration space. The overall algorithm is probabilistically complete and guaranteed to return sound abstractions of configuration spaces for holonomic robots. We evaluated our hierarchical approach based on learned abstractions against state-of-the-art sampling-based and learning-based motion planners on a range of environments. The results show that our approach reduces the time required to compute motion plans by a magnitude of 10 compared to other motion planners.

KEYWORDS

Learning Abstractions for Planning, Deep Learning, Hierarchical Planning, Motion Planning, Learning for Motion Planning

ACM Reference Format:

Naman Shah and Siddharth Srivastava. 2022. Using Deep Learning to Bootstrap Abstractions for Hierarchical Robot Planning. In *Proc. of the 21st International Conference on Autonomous Agents and Multiagent Systems (AAMAS 2022)*, Auckland, New Zealand, May 9–13, 2022, IFAAMAS, 9 pages.

1 INTRODUCTION

Autonomous robots need to be able to efficiently compute long-horizon motion plans for achieving user desired tasks [8, 20, 23]. E.g., consider a scenario where a robot R in a household environment is tasked to reach kitchen K from its current location $B1$ (Fig. 1). State-of-the-art motion planning algorithms such as PRM [13] and RRT [17] use random sampling of low-level configurations to compute a path from the robot’s current location $B1$ to its target location K . Such sampling-based methods fail to efficiently sample configurations from confined spaces such as doorways and corridors under uniform sampling [24].

On the other hand, humans tend to reason using abstract, high-level actions. E.g., in the same scenario, we would use high-level

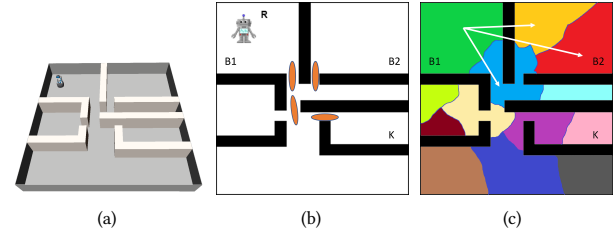


Figure 1: An illustrative environment for a motion planning problem. The robot (R) is tasked to reach the kitchen (K). Orange areas in (b) show a subset of critical regions in the environment. Lastly, (c) shows an example of state abstraction. Each colored cell represents an abstract state. White arrows shows a few abstract actions that takes the robot from one abstract state to another abstract states.

(abstract) actions such as *go out of the room $B1$, pass through the corridor, and enter the kitchen K* . These abstract actions allow us to reason over a long-horizon easily. Currently domain experts need to create such abstractions by hand. This limits the scope and scalability of approaches for hierarchical planning (e.g. [9, 27]) to situations and where domain experts are available and able to correctly intuit the required abstractions.

This paper shows that the required abstractions can be learned by identifying regions in the environment that are important to solve motion planning problems (loosely similar to landmarks in task planning). Molina et al. [24] define such regions as *critical regions*. Critical regions are analogous to *landmarks* in automated planning. Fig. 1(b) shows a few candidate critical regions for the given environment.

In this paper, we investigate two important questions: 1) Can we use deep learning to automatically generate such abstractions for new environments? 2) Can the computed abstractions enable safe and more efficient planning algorithms? The main contributions of this paper are: *a)* a formal foundation for hierarchical (state and action) abstractions based on the critical regions (similar to Fig. 1(c)); *b)* a novel algorithm for on-the-fly construction of such hierarchical abstraction using predicted critical regions; and *c)* a hierarchical multi-source algorithm that utilizes the learned state and action abstractions.

An exhaustive empirical evaluation our approach on a total of twenty different settings with four different robots, which include holonomic and non-holonomic robots, shows that our approach outperforms state-of-the-art sampling-based as well as learning-based motion planners and requires significantly less time to compute

motion plans for holonomic and non-holonomic robots. Our comparison with existing learning-based motion planners shows that generating abstractions and performing hierarchical planning significantly helps in planning. Our thorough empirical results are backed by theoretical results on the completeness and soundness of our approach. Our formal framework provides a way to generate sound abstractions that satisfy *downward refinement property* [1] for holonomic robots.

The rest of the paper is organized as follows: Sec. 2 discusses some of the existing related approaches, Sec. 3 introduces some concepts required to understand our approach, Sec. 4 defines the formal framework for our algorithm, Sec. 5 present our approach and theoretical results in detail. Finally, Sec. 6 presents our extensive empirical evaluation.

2 RELATED WORK

Much of the prior work in on the topic is focused on decomposing the motion planning problem into smaller subproblems to reduce its complexity. Several approaches have been proposed that use state decomposition to reduce the complexity of a motion planning problem. *Vertical cell decomposition* [4] partitions the state space into a collection of vertical cells and computes a roadmap that passes through all of these cells. Brock and Kavraki [2] propose a method that decomposes the overall motion planning problem into multiple subproblems and stitches the solution for each of the subproblems to generate the complete motion plans. They use *wavefront expansion* to compute the decomposition of the state space. While these approaches establish the foundation of decomposition-based motion planning, partitions generated through such approaches are arbitrary and do not provide any guarantees of completeness.

Zhang et al. [32] use rejection sampling to reject unrelated samples to speed up SBMPs. Zhang et al. [32] use reinforcement learning to learn a policy that decides to accept or reject a new sample to expand the search tree. While their approach reduces the search space to compute the path, it still needs to process and samples generated from regions that are irrelevant for the current problem. On the other hand, we use a high-level plan to guide the low-level motion planning which reduces the generation of unnecessary samples. TogglePRM [6] maintains roadmaps for free space and occupied space in the configuration space to estimate the narrow passage and uses this information to sample points from narrow passages. While their approach works well for environments with a certain type of narrow passages, our approach is much more general and produces a high-level abstraction.

Multiple approaches have used statistical learning to boost motion planning. Wang et al. [30] present a comprehensive survey of methods that utilize a variety of learning methods to improve the efficiency of the SBMPs. Multiple approaches discussed by Wang et al. [30] use end-to-end deep learning to low-level reactive policies. End-to-end approaches are attractive given if they succeed, they can compute solutions much faster than traditional approaches, but it is exactly not clear in under which conditions these algorithms would succeed. Formally, these end-to-end deep learning based approaches lack the guarantees about completeness and soundness that our approach provides. Wang et al. [30] also discuss approaches that use learning to aid sampling-based motion planning. We discuss a

few of these approaches that are relevant to this work. Kurutach et al. [16] uses *InfoGAN* [5] to learn state-space partitioning for simple SE^2 robots. While their empirical evaluation shows promising results, similarly to previous decomposition-based approaches, they do not provide any proof of completeness. It is also not clear how their approach would scale to configuration spaces that had more than two dimensions. On the other hand, our approach scales to robots with high DOF and provides formal guarantees of completeness for holonomic robots.

Ichter et al. [11] and Kumar et al. [15] use a conditional variational autoencoder (CVAE) [28] to learn the sampling distribution for the motion planning. Ichter et al. [12] use *betweenness centrality* to learn criticality score for low-level configurations. They uniformly sample a set of configurations from the environment and use configurations with higher criticality to generate a probabilistic roadmap. Their results show significant improvement over vanilla PRM but it is unclear how their approach would perform if environment had regions that are important to compute motion plans yet difficult to sample under uniform sampling. On the other hand, our approach would identify these important regions to overcome such challenges. While all these approaches [11, 12, 15] focus on biasing the sampling distribution towards narrow areas in the environment, our approach aims to build a more general high-level abstraction for the configuration space.

Molina et al. [24] use an image-based approach to learn and infer the sampling distribution using demonstrations. They use top-view images of the environment with *critical regions* highlighted in the image to learn the distribution of critical regions. While Molina et al. [24] develop a method for predicting critical regions and use them with a low-level motion planner, they do not address the key contributions ((a)-(c) in Sec. 1) made by this paper. Specifically, their approach does not use critical regions to learn abstractions and does not perform hierarchical planning. Our empirical results (Sec. 6) that these key contributions are much more effective than a non-hierarchical approach proposed by Molina et al. [24] and yield significant performance in robot planning. Additionally, their approach is restricted to navigational problems and does not scale to configuration spaces with more than two degrees of freedom(DOFs).

Liu et al. [19] use semantic information to bias the sampling distribution for path planning tasks in partially known environments. Compared to Liu et al. [19], our approach is not limited SE^2 configuration space and does not require semantic information explicitly but aims to learn such a notion in the form of critical regions. *SPARK* and *FLAME* [3] use state decomposition to store past experience and use it when queried for similar state decompositions. While their approach efficiently uses the experience from previous iterations, it requires carefully crafted state decompositions in order to cover a large number of scenarios. Whereas our approach generates state abstraction automatically using the predicted critical regions.

3 BACKGROUND

Let $\mathcal{X} = \mathcal{X}_{\text{free}} \cup \mathcal{X}_{\text{obs}}$ be the configuration space of a given robot [18]. Here $\mathcal{X}_{\text{free}}$ represents the set of configurations where the robot is not in collision with any obstacle and \mathcal{X}_{obs} represents configurations in collision with an obstacle. Let $x_i \in \mathcal{X}_{\text{free}}$ and $x_g \in \mathcal{X}_{\text{free}}$

be the initial and goal configurations of the robot, respectively. A motion planning problem is defined as follows:

DEFINITION 1. A motion planning problem \mathcal{M} is defined as a 4-tuple $\langle X, u, x_i, x_g \rangle$, where $X = X_{free} \cup X_{obs}$ is the configuration space and $x_i, x_g \in X_{free}$ are the robot's initial and goal configurations. $u : X \rightarrow \{0, 1\}$ is a collision function that determines collisions for configurations. $u(x) = 1$ iff $x \in X_{obs}$ else 0.

A solution to a motion planning problem is a collision-free trajectory $\tau : [0, 1] \rightarrow X$ such that $\tau(0) = x_i$ and $\tau(1) = x_g$. We abuse the notation to define membership in a trajectory as follows: For a configuration $x \in X$, if there exists a $t \in [0, 1]$ such that $\tau(t) = x$, then $x \in \tau$. A trajectory is collision free if $\forall x \in \tau, u(x) = 0$.

A pair of low-level configuration $x_i, x_j \in X$ is said to be connected iff there exists a collision-free motion plan between x_i and x_j . We define a connectivity function $C : X \times X \rightarrow [0, 1]$ to represent the connectivity for pairs of low-level configurations. $C(x_i, x_j) = 1$ iff x_i and x_j are connected, 0 otherwise.

The presented approach uses *critical regions (CRs)* to learn abstractions. Intuitively, critical regions are regions in the configuration space that have a high density of valid motion plans passing through them for the given class of motion planning problems. Molina et al. [24] define critical regions as follows:

DEFINITION 2. Given a robot R , a configuration space X , and a class of motion planning problems M , the measure of criticality of a Lebesgue-measurable open set $r \subseteq X$, $\mu(r)$, is defined as $\lim_{s_n \rightarrow^+ r} \frac{f(r)}{v(s_n)}$, where $f(r)$ is the fraction of observed motion plans solving tasks from M that pass through s_n , $v(s_n)$ is the measure of s_n under a reference density (usually uniform), and \rightarrow^+ denotes the limit from above along any sequence $\{s_n\}$ of sets containing r ($r \subseteq s_n, \forall n$).

Beam Search. Lowerre [21] introduced beam search as an optimization over breadth-first search (BFS) that explores the state space by expanding only a subset of nodes to compute a path from one to another in the graph. Beam search prunes the fringe to reduce the size of *OPEN* set. We include pseudocode for the beam search in the appendix.

4 FORMAL FRAMEWORK

We begin describing our formal framework with an example. Fig. 1(b) shows a set of critical regions for a given environment. Ideally, we would like to predict these critical regions and generate a state and action abstraction similar to the one shown in Fig. 1(c). The state abstraction shown in Fig. 1(c), similar to a Voronoi diagram, generates cells around each critical region such that the distance from each point in a cell to its corresponding critical regions is less than that from every other critical region. We call this structure a *region-based Voronoi diagram (RBVD)*. Each cell in this region-based Voronoi diagram is considered an abstract state and transitions between these Voronoi cells (abstract states) define abstract actions.

Let ρ be the set of critical regions for the given configuration space X . First we introduce distance metrics d^c and d^r . Here, d^c defines distance between a low-level configuration $x \in X$ and a region $r \in \rho$ such that $d^c(x, r) = \min_{x_i \in r} d(x, x_i)$ and d^r defines the distance between two regions r_1, r_2 such that $d^r = \min_{x_i \in r_1, x_j \in r_2} d(x_i, x_j)$

where d is the euclidean distance. Using these distance metrics, we define region-based Voronoi diagram as follows:

DEFINITION 3. Let $\rho = \{r_1, \dots, r_k\}$ be a set of critical regions for the configuration space X . A region-based Voronoi diagram (RBVD) $\Psi(\rho, X)$ is defined as a set of Voronoi cells ψ_1, \dots, ψ_k such that each Voronoi cell $\psi_i = \{x \in X_{free} | d^c(x, r_i) \leq d^c(x, r_j) \forall 1 \leq j \leq k \wedge j \neq i\}$, $\psi_0 \cup \dots \cup \psi_k = X_{free}$, and $\psi_0 \cap \dots \cap \psi_k = \emptyset$.

We enforce that every Voronoi cell $\psi_i \in \Psi$ is a connected topological space. If a Voronoi cell $\psi_i \in \Psi$ is a disconnected space (due an obstacle), i.e. there exist two or more disjoint sets A_1, \dots, A_j such that $A_1 \cup \dots \cup A_j = \psi_i$, then we decompose ψ_i in additional Voronoi cells $\psi_{i1}, \dots, \psi_{ij}$ such that $\psi_{i1} \cup \dots \cup \psi_{ij} = \psi_i$.

We use notation ψ_r to refer to Voronoi cell ψ corresponding to the critical region r and r_ψ to refer to critical regions r corresponding to the Voronoi cell ψ .

State Abstraction. In this work, we define abstract states using Voronoi cells of an RBVD. Formally, let \mathcal{S} be the set of all abstract states. We define a bijective function $\ell : \Psi \rightarrow \mathcal{S}$ that maps each Voronoi cell of an RBVD to an abstract state. The inverse of this function, ℓ^{-1} maps an abstract state to its corresponding Voronoi cell. We use this to define the state abstraction function α as follows:

DEFINITION 4. Let R be the robot and $X = X_{free} \cup X_{obs}$ be the configuration space of the robot R with set of critical regions ρ . Let $\Psi(\rho, X) = \{\psi_1, \dots, \psi_k\}$ be an RBVD for the robot R , configuration space X , and the set of critical regions ρ and $\mathcal{S} = \{s_1, \dots, s_k\}$ be the set of high-level, abstract states. We define abstraction function $\alpha : X_{free} \rightarrow \mathcal{S}$ such that $\alpha(x) = s$ where $x \in \psi$ and $\ell(\psi) = s$.

We extend this notation to define membership in abstract states as follows: Given a configuration space X and its set of abstract states \mathcal{S} as defined above, a configuration $x \in X_{free}$ is said to be a member of an abstract state $s \in \mathcal{S}$ (denoted $x \in s$) iff $\alpha(x) = s$. We now define adjacency for Voronoi cells in a region-based Voronoi diagram as follows. Recall that C denotes of configurations.

DEFINITION 5. Let ψ_i, ψ_j be Voronoi cells in an RBVD corresponding to critical regions r_{ψ_i} and r_{ψ_j} respectively. Voronoi cells ψ_i and ψ_j are adjacent iff there exist configurations $x_i, x_j \in X_{free}$ such that $C(x_i, x_j) = 1$ and there exists a collision-free trajectory τ between x_i and x_j such that $\forall t \in [0, 1], \tau(t) \in \psi_i$ or $\tau(t) \in \psi_j$.

We extend the above definition to define the neighborhood for an abstract state. Two abstract states $s_i, s_j \in \mathcal{S}$ are neighbors iff $\ell(s_i)$ and $\ell(s_j)$ are adjacent. We now define strong connectivity for abstract states. We use it to ensure that each low-level configuration is reachable from every other low-level configuration in the same abstract state. We define strong connectivity for an abstract state as follows:

DEFINITION 6. A high-level state $s \in \mathcal{S}$ is said to be a strongly-connected state iff for all pairs $(x_i, x_j) \in \ell^{-1}(s) \times \ell^{-1}(s)$, $C(x_i, x_j) = 1$ and there exist a trajectory τ_{ij} such that $\tau(0) = x_i, \tau(1) = x_j$ and $\forall t \in [0, 1], \tau(t) \in s$.

PROPOSITION 1. Let \mathcal{S} be the set of abstract states corresponding to the set of critical regions ρ for robot R and configuration space X . If R is a holonomic robot then every state $s \in \mathcal{S}$ is strongly connected.

PROOF. Let $\Psi(\rho, \mathcal{X})$ be the RBVD for the set of critical regions ρ corresponding the set of abstract states \mathcal{S} . Given each Voronoi cell $\psi \in \Psi$ is a connected space, there would exist a trajectory between each pair of configurations in the Voronoi cell for holonomic robots. This makes each abstract state $s \in \mathcal{S}$ strongly connected. \square

We define abstract actions as transition between abstract states. Let \mathcal{S} be the set of abstract states. We define the set of abstract actions \mathcal{A} using \mathcal{S} be such that $\mathcal{A} = \{a_{ij} | \forall (s_i, s_j) \in \mathcal{S} \times \mathcal{S}\}$. An action $a_{ij} \in \mathcal{A}$ is applicable iff there exist abstract states $s_i, s_j \in \mathcal{S}$ such that $s_j = a_{ij}(s_i)$ and s_i and s_j are neighbors.

We use this formulation of the region-based Voronoi diagrams and state abstraction to prove the soundness of the abstraction.

THEOREM 4.1. *Let \mathcal{X} be a configuration space and ρ be the set of critical regions for \mathcal{X} . Let Ψ be the RBVD for the critical regions ρ and the configuration space \mathcal{X} and let \mathcal{S} be the set of abstract states corresponding to Ψ . Let x_0 and x_g be the initial and goal configurations of the robot. If every state $s \in \mathcal{S}$ is strongly connected and there exists a sequence of abstract states $P = \langle s_{\psi_0}, \dots, s_{\psi_g} \rangle$ such that $x_0 \in s_{\psi_0}$, $x_g \in s_{\psi_g}$, and all consecutive states $s_{\psi_i}, s_{\psi_{i+1}} \in P$ are neighbors, then there exists a motion plan from x_0 to x_g such that $\tau(0) = x_0$, $\tau(1) = x_g$, and $\forall x_i \in \tau, x_i \in s_{\psi_k}$ such that $s_{\psi_k} \in P$.*

PROOF. For two consecutive abstract states $s_i, s_{i+1} \in P$ let $\psi_i, \psi_{i+1} \in \Psi$ be Voronoi cells such that $\ell^{-1}(s_i) = \psi_i$ and $\ell^{-1}(s_{i+1}) = \psi_{i+1}$. If s_i and s_{i+1} are neighbors, then according to Def. 5 there exists a pair of low-level configurations $x_i, x_{i+1} \in \mathcal{X}$ such that there exists a collision free trajectory between x_i to x_{i+1} . Given all abstract states are strongly connected, we can say that for every low-level configurations $x_j \in s_i$, there exists a collision-free trajectory between x_j and x_i and there for every low-level configurations $x_k \in s_{i+1}$, there exists a collision-free trajectory between x_k and x_{i+1} . This implies that there exists a motion plan between each pair of configurations in s_{ψ_i} and $s_{\psi_{i+1}}$. Therefore, if we consider this for each subsequent pair of abstract states in P , we can say that there exist a motion plan τ from x_0 to x_g such that $\tau(0) = x_0$, $\tau(1) = x_g$, and $\forall x_i \in \tau, x_i \in s_{\psi_k}$ such that $s_{\psi_k} \in P$. \square

5 OUR APPROACH

Our overall approach can be divided into main phases: 1) Learning to predict critical regions in a given configuration space and 2) using these regions to derive state and action abstractions. First, we discuss how we bootstrap abstractions and compute motion plans using the predicted critical regions, and then we present our approach for learning a model that predicts the critical regions.

5.1 Bootstrapping Abstraction

In this section, we describe our approach – *hierarchical abstraction-guided robot planner (HARP)* – to generate abstract states and actions and use them to efficiently perform hierarchical planning. A naïve approach would be to generate a complete RBVD and then extract abstract states and actions from it. This would require iterating over all configurations in the configuration space and computing a large number of motion plans to identify executable abstract actions. This is expensive (and practically infeasible) for continuous low-level configuration spaces. Instead, we use the RBVD as an

Algorithm 1: Hierarchical Abstraction-guided Robot Planner (HARP)

Input: Configuration space \mathcal{X} , a region predictor Φ , an initial configuration $x_0 \in \mathcal{X}$, goal configuration $x_g \in \mathcal{X}$, a custom heuristic h , low-level sampling-based motion planner MP

Output: A motion plan τ

```

1  $\rho \leftarrow \text{predict\_critical\_regions}(\Phi, \mathcal{X}, x_0, x_g)$ 
2  $\mathcal{S}, \mathcal{A} \leftarrow \text{generate\_state\_action\_abstractions}(\rho, \mathcal{X})$ 
3  $s_0, s_g \leftarrow \text{get\_HL\_state}(\mathcal{S}, \rho, x_0), \text{get\_HL\_state}(\mathcal{S}, \rho, x_g)$ 
4  $P \leftarrow \text{multi\_source\_bi\_directional\_beam\_search}(\mathcal{S}, \mathcal{A}, s_0, s_g)$ 
5  $\tau \leftarrow \text{refine\_path}(P, MP)$ 
6  $h \leftarrow \text{update\_heuristic}(\tau, \mathcal{S})$ 
7 return  $\tau$ 
```

implicit concept. We compute membership of low-level configurations in abstract states only when needed and initially consider every action in the set \mathcal{A} to be applicable. This reduces the time required to generate abstract states and actions while trading off the soundness of generated abstractions.

Vanilla high-level planning using the set of all abstract actions $\tilde{\mathcal{A}}$ would be inefficient as it may yield plans for which low-level refinement may not exist as we do not know the applicability of these abstract actions at low-level. To overcome this challenge, we develop a hierarchical multi-source bi-directional planning algorithm that performs high-level planning from multiple abstract states. Generally, a multi-source approach would not work for robot planning in the absense of any prior knowledge of the intermediate states. In this case, use of critical regions as abstract intermediate states permits the efficient use of a multi-source search. Our high-level planner generates a set of candidate high-level plans from the abstract initial state to the abstract goal state using a custom heuristic (which is continually updated). These paths are then simultaneously refined by the low-level planner to compute a trajectory from the initial low-level configuration to the goal configuration while updating the heuristic function.

Algorithm 1 describes our overall approach. Given the configuration space \mathcal{X} and initial and goal configurations (x_0 and x_g) of the robot, HARP uses a learned DNN Φ to generate a set of critical regions ρ (Sec. 5.2 discusses how we learn this model Φ) (line 1). HARP uses this set of identified critical regions ρ to generate the set of abstract states \mathcal{S} and actions \mathcal{A} (line 2). Our overall algorithm can be broken down into three important steps: 1) Computing a set of candidate high-level plans, 2) Refining candidate high-level plans into a low-level trajectory, and 3) Updating the heuristic for abstract states. We now explain each of these steps in detail.

Computing a High-Level Plan. The first step in Algorithm 1 is computing a high-level plan from the initial configuration x_0 to the goal configuration x_g . First, we determine abstract initial and goal states s_0 and s_g corresponding to the initial and goal configurations x_0 and x_g (line 3). We store sampled points from each critical region in a k-d-tree and query it to determine the abstract state for the given low-level configurations without explicitly constructing

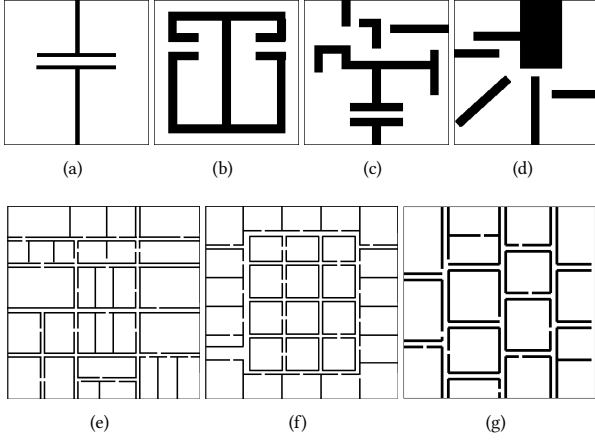


Figure 2: Test environments for our approach. Dimensions of environments (a)-(d) are $5m \times 5m$ and dimensions of environments (e)-(g) are $25m \times 25m$.

the complete RBVD. This allows us to dynamically and efficiently determine high-level states for low-level configurations.

Once we determine initial and goal states s_0 and s_g , we use our high-level planner to compute a set of candidate high-level plans going from s_0 to s_g (line 4). To compute these candidate high-level plans, we develop a multi-source bi-directional variant of beam search [21] that yields multiple high-level candidate plans. We call this *multi-source bi-directional beam search*. We include the pseudocode for vanilla and multi-source bi-directional beam search in the appendix.

Intuitively the algorithm works as follows: To allow beam search to start from multiple abstract states, we initiate the fringe of the beam search with multiple randomly sampled abstract states. We expand these states towards the initial state and goal state. We use actions $a_i \in \mathcal{A}$ to generate all successors of the node to be expanded (in this case, all abstract states) and add them to the fringe. We expand top- k abstract states from the fringe and discard the rest. This allows our approach to handle a large number of abstract actions for each abstract state. We use a custom heuristic to determine to rank abstract states in the fringe. We use a combination of the estimated distance between two high-level states and the estimated distance between the given state and the initial and goal states as the heuristic function for the beam search to allow it to act as a bi-directional search. Formally speaking, we define the heuristic function for an abstract state s_j as follows:

$$h(s_j) = h'(s_k, s_j) + \min\{h'(s_j, s_i), h'(s_j, s_g)\}$$

Here s_k is the abstract state being expanded, s_j is the successor of s_k , and s_i and s_g are initial and goal abstract states. $h'(s_j, s_k) = \epsilon_{jk} d^r(r_j, r_k)$ defines the estimated distance between abstract high-level states s_j and s_k . Here, r_j and r_k are the critical regions corresponding to the high-level states s_j and s_k respectively. $\epsilon_{jk} \in (0, 1]$ is a constant that our algorithm dynamically updates (explained later). We start with $\forall j, k \epsilon_{jk} = 1$. This custom heuristic function allows the abstract state to expand in both directions and take into the account estimation of the action costs which are not precisely

known due to abstraction. We use a priority queue to maintain the order of states in the fringe and select them for expansion and compute these priorities using the heuristic function h . Vanilla beam search terminates when it finds a plan that reaches the goal state. Instead, multi-source bi-directional beam search continues to compute plans until it computes k plans or fringe gets empty.

Once we generate a set of candidate high-level plans from multi-source bi-directional beam search, we use a low-level planner to refine these plans into a low-level collision-free trajectory from initial low-level configuration x_0 to goal configuration x_g (line 5).

Refining High-level Plans. While any *probabilistically complete* motion planner can be used to refine the high-level plan into a low-level trajectory between given two configurations, we use *Learn and Link Planner (LLP)* [24] in HARP as it allows us to easily use the abstract states and their critical regions to efficiently compute motion plans. LLP is a sampling-based motion planner that initializes exploration trees rooted at N samples from the configuration space and extends these exploration trees until they connect and form a single tree. Once a single tree is formed, the planner uses Dijkstra's Algorithm [7] to compute a path from the initial state to the goal state.

In order to use LLP to refine a set of candidate high-level plans simultaneously, we first select a subset of critical regions $\bar{\rho} \subseteq \rho$ that includes critical regions corresponding to all high-level states visited in candidate plans. We use this subset of critical regions $\bar{\rho}$ to provide initial samples to LLP to initialize exploration trees. In this work, we generate αN samples from the set of critical regions, and the rest of the $(1 - \alpha)N$ samples are generated uniformly random for some $\alpha \in (0, 1)$. To expand these exploration trees, we generate first λ samples from the set critical regions ρ and then continue with uniform sampling.

Updating the Heuristic Function. When a low-level trajectory τ is computed, we use it to update the heuristic function h for high-level planning (line 6). We compute the abstraction $\bar{\tau}$ of the low-level solution trajectory τ . For each consecutive pair of abstract states $\langle s_j, s_k \rangle$ in $\bar{\tau}$, we decrease the value of the constant ϵ_{jk} . This allows HARP to use experience from previously computed trajectories to prioritize abstract actions that have low-level refinements and compute more accurate high-level plans.

We use these characteristics of our algorithm to show that our approach is *probabilistic complete*.

THEOREM 5.1. *If low-level motion planner (MP in Alg. 1) is probabilistically complete, then HARP is probabilistically complete.*

PROOF. (Sketch) While refining high-level plans to low-level motion plan (line 5 in Alg. 1), HARP uses a finite number of samples from the critical regions along the high-level plans to initialize low-level motion planner. This does not reduce the number of configurations with a non-zero probability of being sampled in refinement process which makes HARP probabilistically complete. \square

5.2 Learning to Predict Critical Regions

We now present our approach for learning a model Φ that learns to predict critical regions for the given environment. We explain how our approach is able to generate a robot-specific architecture of the

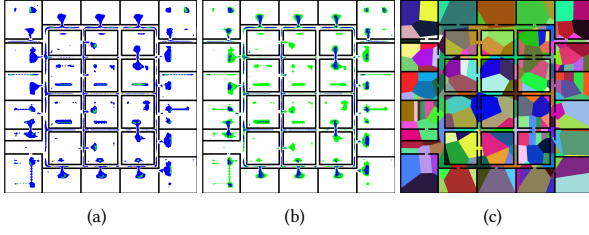


Figure 3: Test evaluations for an 4-DOF hinged robot. (a) and (b) shows the CRs predicted by the model for the. Blue regions in (a) show that model predicted the robot’s base link to be horizontal while green regions show that the model predicted the robot’s base link to be vertical. Blue regions in (b) show that the network predicted the hinge to be closer to 180° and green regions show that the network predicted it to be closer to 90° or 270°. (c) shows state abstraction generated by our approach.

network. We include specifics about data generation and network training in the appendix.

Deriving Robot Specific Network Architectures. We use the number of DOFs of the robot and the robot geometry to derive the UNet-based [25] architecture as follows:

We use a standard fully convolutional UNet architecture that consists of a total of sixteen layers. The first eight d -dimensional convolutional layers work as an encoder unit and the remaining eight d -dimensional deconvolutional layers work as a decoder unit. We use the geometry of the robot’s links to determine the value d . E.g., $d = 2$ for robots with 2D links. We show network architecture in the appendix for convenience. We use a single channel of the last layer of the base architecture to predict critical locations for the end-effector (base link for path planning) in the environment. We use additional k convolutional layers to predict the distribution for joint values where k represents the number of degrees of freedom of the robot that is not captured by the location of the end-effector in the environment. E.g., for the robot that has four degrees of freedom (x, y, θ, ω) where x and y represents the location of the robot in the environment, the network would have $k = 2$ additional convolutional layers - one convolutional layer for each remaining degree of freedom.

The dimensions of input to the network are computed using the dimensionality of the environment and the number of degrees of freedom of the robot. The first channel in the input represents the occupancy matrix of the environment and each additional channel represents the goal value for each DOF of the robot. So, for a 4-DOF robot, the network will have five channels in the input layer.

The total number of channels in a label vector is also computed using the DOFs of the robot. We discretize the values of each joint of the robot in p discrete bins. We use a single channel to represent the distribution of critical regions for the end-effector. Additional p channels represent the distribution for the values of each joint. E.g., for a robot with four DOF (x, y, θ, ω) , the total number of output channels would be equal to 21, if $p = 10$ for θ and ω .

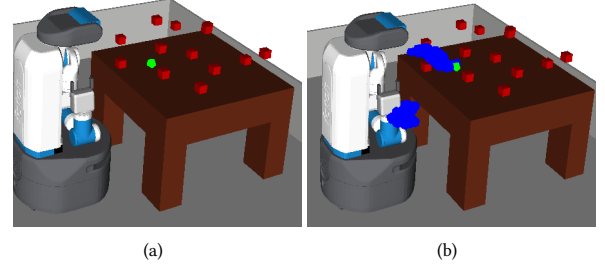


Figure 4: Test evaluations for arm manipulation tasks using 8-DOF Fetch. The green region in (a) shows the goal location for the end effector. (b) shows the critical regions generated by the learned model. Although the network predicts CRs for all the joints, only CRs for end-effector’s location are shown.

6 EMPIRICAL EVALUATION

We extensively evaluate our approach in twenty different scenarios with four different robots. All experiments were conducted on a system running *Ubuntu 18.04* with 8-core *i9* processor, 32 GB RAM, and an *Nvidia 2060* GPU (our approach uses only a single core). We compare our approach with state-of-the-art motion planners such as *RRT* [17], *PRM* [13], and *BiRRT* [14]. As LLP is implemented using *Python*, we use the *Python* implementation of the baseline algorithms available at <https://ompl.kavrakilab.org/> for comparison. Our training data, code, trained model, and results are available in the appendix. It also includes parameters that we used to generate data for every setup.

3-DOF Rectangular Robot. For the first set of experiments, the objective is to solve motion planning problems for a 3-DOF rectangular robot. The robot can move along the x and y axes and it can rotate around the z axis.

3-DOF Non-Holonomic Rectangular Car Robot. For the second set of experiments, we evaluated our approach with a rectangular non-holonomic robot similar to a simple car. Controls available to operate the robot were linear velocity $v \in [-0.2, 0.2]$ and the steering angle $\theta \in [-\frac{\pi}{4}, \frac{\pi}{4}]$ while three degrees of freedom (location along x -axis, location along y -axis, and rotation around z -axis) were required to represent the robot’s transformation.

4-DOF Hinged Robot. For the third set of experiments, we used a robot with a hinge joint to evaluate our approach. The robot’s 4 DOFs are its location along x and y axes, rotation along z -axis (θ), and the hinge joint (ω) with the range $[-\frac{\pi}{2}, \frac{\pi}{2}]$.

8-DOF Fetch Robot. For the last set of experiments, we used our approach with a mobile manipulator named Fetch [31] to perform arm manipulation. The goal of this experiment is to evaluate the scalability of our approach to robots with high degrees of freedom.

Figures 2 and 4 show the test environments (completely unseen by the model while training) for our system. Environments shown in Fig. 2 are inspired by the indoor office and household environments. Our training data consisted of environments similar to the

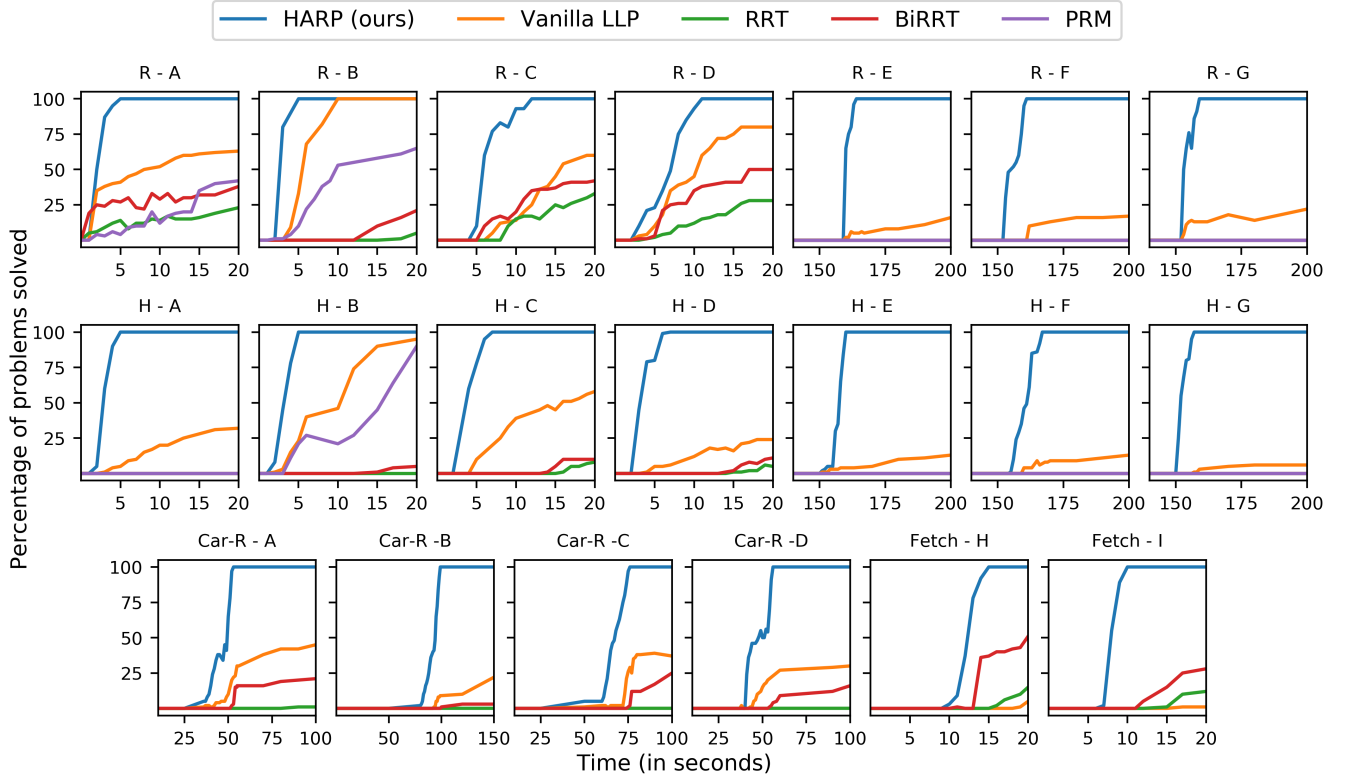


Figure 5: Each plot shows the fraction of 100 independently generated motion planning tasks solved (y-axis) in the given time (x-axis) for all the test environments and robots. The title of each subplot represents the robot and the environment. E.g., “R - A” stands for rectangular robot in environment A (Fig. 2(a)). Similarly, “H” stands for the hinged robot and “Car-R” stands for rectangular the car robot.

ones shown in Figures 2(a)-(d) with dimensions $5m \times 5m$. We investigate scalability of our approach by conducting experiments in environments shown in Fig. 2(e) through 2(g) with dimensions $25m \times 25m$ (much larger than training environments). To handle such large environments without making any changes to the DNN, we use the standard approach of sliding windows with stride equal to window-width [10, 22, 26, 29]. This crops the larger environment into pieces of the size of training environment. Individual predictions are then combined to generate set of critical regions for arbitrary large environments. We also evaluate the applicability of our approach to non-holonomic robots in environments shown in Fig. 2(a) through (d).

6.1 Analysis of the Results

As discussed in the introduction (Sec. 1, our objective is to show whether 1) state and action abstractions can be derived automatically and 2) whether auto-generated state and action abstractions can be efficiently used in a hierarchical planning algorithm. Additionally, we also investigate 3) does dynamically updating the heuristic function (line 6 in Alg. 1) improve efficiency?

a) Can We Learn State and Action Abstractions? Our approach learns critical regions for each DOF of the robot. Fig. 3 shows critical regions predicted by our learned model. We can see that our model was able to identify critical regions in the environment such as doorways and narrow hallways. Fig. 3(a) shows critical regions for orientation of the robot for SE^3 robots (captured by DOF θ). The blue regions in the figure represent the horizontal orientation of the robot and the green regions represent the vertical orientation of the robot. Fig. 3(b) shows critical regions for the hinge joint ω for the SE^3 robot. Blue regions show that the network predicted the hinge joint to be flat (close to 0°) and green regions represent configurations where the model predicted “L” configurations of the robot (ω close to 90° or 270°). Fig. 3 shows that our approach was able to predict the correct orientation of the robot accurately most of the time. Our approach was able to scale to robots with a high number of degrees of freedom. Fig. 4(a) shows one of the test environments used for these experiments and Fig. 4 (b) shows the critical regions predicted by the learned model. This shows that our model was able to learn critical regions in the environment that can be used to generate efficient abstractions. We include similar results for other environments in the appendix.

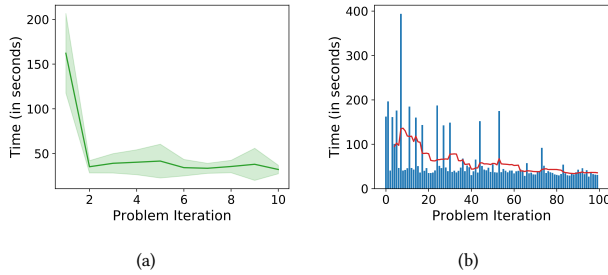


Figure 6: (a) Solving 20 randomly generated problems repeatedly 10 times. X-axis show the problem iteration and y-axis shows the average time over 20 problem instances. (b) Time taken to solve 100 randomly generated problem instances. X-axis shows the problem number and y-axis shows the taken to solve each problem.

Now we answer the second question that whether using abstractions to compute motion plans helps improve the planner efficiency by qualitatively comparing our approach with a few existing sampling-based motion planners.

b) Can Learned Abstractions be Used Efficiently for Hierarchical Planning? We compare our approach against widely used sampling-based motion planners such as RRT [17], PRM [13], and BiRRT [14].

Fig. 5 shows the comparison of our approach with other sampling-based motion planners. The x-axis shows the time in seconds and the y-axis shows the percentage of 100 independently generated motion planning problems solved in that time. We generate a new batch of 100 random test problems for each timestep to thoroughly test our approach and reduce statistical inconsistencies. We can clearly see from Fig. 5 that our approach significantly outperforms all of the existing sampling-based motion planners. Specifically for environments *C*, *D*, and *E* uniform sampling-based approaches were not able to solve a single problem for a time threshold of 600s.

Our approach also outperforms the learning-based planner Vanilla LLP [24] (Fig. 5), which uses learned critical regions but does not use state and actions and does not perform hierarchical planning. This illustrates value of learning abstraction and using them efficiently for hierarchical planning.

Similarly, We also evaluate our approach against TogglePRM [6]. TogglePRM is written in C++ and accepts only discrete SE^2 configuration space for a simple dot robot. We created discrete variants of environments shown in Fig. 2(a) and 2(b) with a total of 50176 states and compare the total number of nodes sampled. For 100 random trials, on an average our approach generated 631 ± 278 and 496 ± 175 states compared to TogglePRM which generates 4234 ± 532 and 19234 ± 4345 states for discrete variants of the environments shown in Fig. 2(a) and 2(b) respectively. Our approach was able to outperform TogglePRM since these environments do not have α - ϵ -separable passages [6].

c) Does Dynamically Updating Heuristic Function Improve Efficiency? To answer this question, we carried out two sets of experiments. In the first set of experiments, we generated 20 random

motion planning problems and solved each problem repeatedly for 10 times while updating the heuristic function. We maintained separate copies of high-level heuristic functions for each problem. Fig. 6(a) shows the results for this set of experiments in the environment *E* (Fig. 2(e)) with the 4-DOF hinged robot. The x-axis shows the planning iteration and the y-axis shows the average time over randomly generated 20 problem instances. We can see how planning time reduces drastically once costs for abstract actions are updated.

In the second set of experiments, we generated 100 random pairs of initial and goal states and computed motion plans for each of them. This time, we maintained the heuristic function across all problems and updated it after each motion planning query. Fig. 6(b) shows the results for this experiment in the environment *E* (Fig. 2(e)) with the 4-DOF hinged robot. The x-axis shows the problem number and the y-axis shows the time taken by our approach to compute a solution. The red line in the plot shows the moving average of planning time. We can see in Fig. 6(b) that dynamically updating the heuristic function for high-level planning helps to increase the efficiency of HARP.

Empirical evaluation using these experiments clearly validates our hypothesis that effectively using abstraction improves motion planning efficiency.

7 CONCLUSION

In this paper, we presented a probabilistically complete approach HARP, that uses deep learning to identify abstractions for the input configuration space. It learns state and action abstractions in a bottom-up fashion and uses them to perform efficient hierarchical robot planning. We developed a new multi-source bi-directional planning algorithm that uses learned state and action abstraction along with a custom dynamically maintained cost function to generate high-level plans. A low-level motion planner refines these high-level plans into a trajectory that achieves from the initial to the goal configuration.

Our formal framework provides a way to generate sound abstractions that satisfy the downward refinement property for holonomic robots. Our empirical evaluation on a large variety of problem settings shows that our approach is able to significantly outperform state-of-the-art sampling-based motion planners. Through our empirical evaluation, we show that our approach is robust and can be scaled to large environments and to robots that have high degrees of freedom. Our work presents a foundation for learning high-level, abstract actions from low-level trajectories. Currently, our approach works for deterministic robot planning problems. We aim to extend our approach to support stochastic settings and learn abstractions for combined task and motion planning problems.

ACKNOWLEDGMENTS

We thank Abhyudaya Srinet for his help in implementing an primitive version of the presented work. We thank Kyle Atkinson for his help with creating test environments. This work is supported in part by the NSF under grants 1909370 and 1942856.

REFERENCES

- [1] Fahiem Bacchus and Qiang Yang. 1991. The Downward Refinement Property.. In *Proc. IJCAI*, 1991.

- [2] O. Brock and L.E. Kavraki. 2001. Decomposition-based motion planning: a framework for real-time motion planning in high-dimensional configuration spaces. In *Proc. ICRA*, 2001).
- [3] Constantinos Chamzas, Zachary Kingston, Carlos Quintero-Peña, Anshumali Shrivastava, and Lydia E Kavraki. 2020. Learning Sampling Distributions Using Local 3D Workspace Decompositions for Motion Planning in High Dimensions. *arXiv preprint arXiv:2010.15335* (2020).
- [4] Bernard Chazelle. 1985. Approximation and decomposition of shapes. *Algorithmic and Geometric Aspects of Robotics 1* (1985), 145–185.
- [5] Xi Chen, Yan Duan, Rein Houthoofd, John Schulman, Ilya Sutskever, and Pieter Abbeel. 2016. Infogan: Interpretable representation learning by information maximizing generative adversarial nets. In *Proc. NeurIPS*, 2016.
- [6] Jory Denny and Nancy M. Amato. 2013. Toggle PRM: A Coordinated Mapping of C-Free and C-Obstacle in Arbitrary Dimension. *Algorithmic Foundations of Robotics X. Springer Tracts in Advanced Robotics (STAR)* 86 (2013), 297–312. https://doi.org/doi.org/10.1007/978-3-642-36279-8_18 Presented at the 2012 Workshop on the Algorithmic Foundations of Robotics (WAFR).
- [7] Edsger W Dijkstra. 1959. A note on two problems in connexion with graphs. *Numerische mathematik* 1, 1 (1959), 269–271.
- [8] Paul Duckworth, Yiannis Gatsoulis, Ferdian Jovan, Nick Hawes, David C Hogg, and Anthony G Cohn. 2016. Unsupervised learning of qualitative motion behaviours by a mobile robot. In *Proceedings of the 2016 International Conference on Autonomous Agents & Multiagent Systems*. 1043–1051.
- [9] Caelan Reed Garrett, Tomás Lozano-Pérez, and Leslie Pack Kaelbling. 2020. PDDL-Stream: Integrating symbolic planners and blackbox samplers via optimistic adaptive planning. In *Proceedings of the International Conference on Automated Planning and Scheduling*, Vol. 30. 440–448.
- [10] Le Hou, Dimitris Samaras, Tahsin M Kurc, Yi Gao, James E Davis, and Joel H Saltz. 2016. Patch-based convolutional neural network for whole slide tissue image classification. In *Proceedings of the IEEE conference on computer vision and pattern recognition*. 2424–2433.
- [11] Brian Ichter, James Harrison, and Marco Pavone. 2018. Learning sampling distributions for robot motion planning. In *Proc. ICRA*, 2018.
- [12] Brian Ichter, Edward Schmerling, Tsang-Wei Edward Lee, and Aleksandra Faust. 2020. Learned Critical Probabilistic Roadmaps for Robotic Motion Planning. In *2020 IEEE International Conference on Robotics and Automation (ICRA)*. 9535–9541. <https://doi.org/doi.org/10.1109/ICRA40945.2020.9197106>
- [13] Lydia E Kavraki, Petr Svestka, J-C Latombe, and Mark H Overmars. 1996. Probabilistic roadmaps for path planning in high-dimensional configuration spaces. *IEEE transactions on Robotics and Automation* 12, 4 (1996), 566–580.
- [14] James J Kuffner and Steven M LaValle. 2000. RRT-connect: An efficient approach to single-query path planning. In *Proceedings 2000 ICRA. Millennium Conference. IEEE International Conference on Robotics and Automation. Symposia Proceedings (Cat. No. 00CH37065)*, Vol. 2. IEEE, 995–1001.
- [15] Rahul Kumar, Aditya Mandalika, S. Choudhury, and S. Srinivasa. 2019. LEGO: Leveraging Experience in Roadmap Generation for Sampling-Based Planning. *Proc. IROS*, 2019 (2019).
- [16] Thanard Kurutach, Aviv Tamar, Ge Yang, Stuart Russell, and Pieter Abbeel. 2018. Learning plannable representations with causal infogan. *arXiv preprint arXiv:1807.09341* (2018).
- [17] Steven M LaValle. 1998. Rapidly-exploring random trees: A new tool for path planning. (1998).
- [18] S. M. LaValle. 2006. *Planning Algorithms*. Cambridge University Press, Cambridge, U.K. Available at <http://planning.cs.uiuc.edu/>.
- [19] K. Liu, M. Stadler, and N. Roy. 2020. Learned Sampling Distributions for Efficient Planning in Hybrid Geometric and Object-Level Representations. In *Proc. ICRA*, 2020.
- [20] Shih-Yun Lo, Shiqi Zhang, and Peter Stone. 2018. PETLON: planning efficiently for task-level-optimal navigation. In *Proceedings of the 17th International Conference on Autonomous Agents and MultiAgent Systems*. 220–228.
- [21] Bruce T Lowerre. 1976. *The harpy speech recognition system*. Carnegie Mellon University.
- [22] Xin Lu, Zhe Lin, Xiaohui Shen, Radomir Mech, and James Z Wang. 2015. Deep multi-patch aggregation network for image style, aesthetics, and quality estimation. In *Proceedings of the IEEE international conference on computer vision*. 990–998.
- [23] Matteo Luperto, Luca Fochetta, and Francesco Amigoni. 2020. Exploration of indoor environments predicting the layout of partially observed rooms. *arXiv preprint arXiv:2004.06967* (2020).
- [24] Daniel Molina, Kislay Kumar, and Siddharth Srivastava. 2020. Identifying Critical Regions for Motion Planning using Auto-Generated Saliency Labels with Convolutional Neural Networks. *Proc. ICRA*, 2020 (2020).
- [25] O. Ronneberger, P.Fischer, and T. Brox. 2015. U-Net: Convolutional Networks for Biomedical Image Segmentation. In *Medical Image Computing and Computer-Assisted Intervention (MICCAI) (LNCS, Vol. 9351)*. Springer, 234–241. <http://lmb.informatik.uni-freiburg.de/Publications/2015/RFB15a> (available on [arXiv:1505.04597 \[cs.CV\]](https://arxiv.org/abs/1505.04597)).
- [26] Taibou Birgui Sekou, Moncef Hidane, Julien Olivier, and Hubert Cardot. 2019. From Patch to Image Segmentation using Fully Convolutional Networks–Application to Retinal Images. *arXiv preprint arXiv:1904.03892* (2019).
- [27] Naman Shah, Deepak Kala Vasudevan, Kislay Kumar, Pranav Kamojjhala, and Siddharth Srivastava. 2020. Anytime integrated task and motion policies for stochastic environments. In *2020 IEEE International Conference on Robotics and Automation (ICRA)*. IEEE, 9285–9291.
- [28] Kihyuk Sohn, H. Lee, and Xinchun Yan. 2015. Learning Structured Output Representation using Deep Conditional Generative Models. In *Proc. NIPS*, 2015.
- [29] Chaohui Tang, Qingxin Zhu, Wenjun Wu, Wenlin Huang, Chaoqun Hong, and Xinzhen Niu. 2020. PLANET: improved convolutional neural networks with image enhancement for image classification. *Mathematical Problems in Engineering* 2020 (2020).
- [30] Jiankun Wang, Tianyi Zhang, Nachuan Ma, Zhaoting Li, Han Ma, Fei Meng, and Max Q-H Meng. 2021. A survey of learning-based robot motion planning. *IET Cyber-Systems and Robotics* (2021).
- [31] Melonee Wise, Michael Ferguson, Derek King, Eric Diehr, and David Dymesich. 2016. Fetch and freight: Standard platforms for service robot applications. In *Workshop on Autonomous Mobile Service Robots*.
- [32] Clark Zhang, Jinwook Huh, and Daniel D Lee. 2018. Learning implicit sampling distributions for motion planning. In *Proc. IROS*, 2018.